Enclosure, Attachment 1

1CAN082004

Dominion Engineering, Inc.

"Circumferential Crack Growth Evaluation for ANO-1 HPI Nozzle "D" Dissimilar Metal Weld," DEI Calculation C-4728-00-03, Rev. 0, dated August 4, 2020
(32 pages)

RECORD OF REVISIONS

Rev.	Description	Prepared by Date	Checked by Date	Reviewed by Date	Approved by Date
0	Original Issue	K.J. Fuhr 8/4/2020	M. Burkardt Aug. 4, 2020	M. Burkardt Aug. 4, 2020	G.A. White 8/4/2020
		K.J. Fuhr Senior Engineer	M. Burkardt Senior Engineer	M. Burkardt Senior Engineer	G.A. White Principal Engineer

The last revision number to reflect any changes for each section of the calculation is shown in the Table of Contents. The last revision numbers to reflect any changes for tables and figures are shown in the List of Tables and the List of Figures. Changes made in the latest revision, except for Rev. 0 and revisions which change the calculation in its entirety, are indicated by a double line in the right hand margin as shown here.

TABLE OF CONTENTS

LIST OF TABLES

LIST OF FIGURES

1 PURPOSE

The dissimilar metal weld (DMW) in the high pressure injection (HPI) nozzles at Arkansas Nuclear One, Unit 1 (ANO-1) are fabricated using Alloy 82/182 weld material, which is susceptible to degradation due to primary water stress corrosion cracking (PWSCC). The DMW in HPI nozzle P32D on loop A2 (HPI nozzle D) was replaced following the detection of an indication in the thermal sleeve/safe end material by PT during operation in 1982 [1]. The configuration of the HPI nozzle and its single-V dissimilar metal weld are shown in Figure 1 and Figure 2, respectively. The HPI nozzles at ANO-1 are subject to periodic ultrasonic examinations per ASME Code Case N-770-5 [2], as mandated and conditioned by 10 CFR 50.55a(g)(6)(ii)(F). This code case requires that a volumetric examination be performed of unmitigated cold-leg butt weld locations at operating temperature $\geq$525°F and <580°F, less than NPS 14 (Inspection Item B-1) such as the ANO-1 HPI nozzles every second inspection period (as defined by ASME Section XI), not to exceed 7 years.

This calculation provides a technical basis for a one-time alternative volumetric reexamination interval for the ANO-1 HPI nozzle D. Specifically, the crack growth calculation demonstrates the acceptability of a volumetric reexamination interval of nominally 7.5 years.

2 SUMMARY OF RESULTS

A circumferential crack growth evaluation was performed considering the specific geometry and loads applicable to the ANO-1 HPI nozzle D dissimilar metal weld, including the weld residual stress (WRS) analysis results documented in C-4728-00-01, Rev. 0 [3]. The crack growth calculations applied the common deterministic approach for unmitigated Alloy 82/182 dissimilar metal piping butt welds in PWRs. The results of these crack growth calculations demonstrate the acceptability of the alternative volumetric reexamination interval (nominally 7.5 years) by demonstrating that the alternative interval is sufficient to provide reasonable assurance of the structural integrity of the ANO-1 HPI nozzle D. Hence, the alternative examination interval provides an acceptable level of quality and safety.

The key results of the crack growth calculations are as follows:

- The limiting case for the calculated time for a circumferential crack to grow from 10% through-wall to the allowable depth of 75% through-wall—as documented in C-4728-00-02, Rev. 0 [4]—is 14.6 years. In this worst-case, an additional 1.2 years is calculated for the crack to penetrate through the remaining 25% of the wall thickness.

- None of the cases evaluated that grow through-wall without arresting result in a flaw growing longer than the maximum allowable flaw length for a depth of 75% through-wall before reaching 75% through-wall. As documented in C-4728-00-02, Rev. 0 [4], the maximum allowable flaw length for a 75% through-wall flaw is 45% of the circumference.

3 INPUT REQUIREMENTS

The following inputs were used in support of this calculation:

1. The nominal geometry of the HPI nozzle and original safe end is provided in Reference [6.g], with details for the modified configuration of HPI nozzle D in References [6.f], [6.h], and [7.a]. The relevant dimensions for the crack growth calculation are as follows:
   a. Nozzle and safe end inner diameter (ID) at dissimilar metal weld prep, nominal: 2.063 in. [7.a, Page 45 and 50])
   b. Nozzle and safe end outer diameter (OD), nominal: 3.5 in. ([6.f] and [6.h])
   c. Angle of V-groove for DMW, nominal: 30° [7.a, Page 45 and 50]
   d. Width of DMW at root, nominal: 0.125 in. [7.a, Pages 45-50]
   e. Minimum buttering thickness: 3/16 in. [7.a, Page 45]
   f. Distance from centerline of DMW to centerline of stainless steel weld: 5.188 in. [7.a, Pages 45-50]
2. As-built dimensions for HPI nozzle D and its DMW are provided in Reference [8]. The relevant dimensions for the crack growth calculation are as follows:
   a. Minimum wall thickness, as-built: 0.68 in. [8, Dimension T3 for centerline of DMW]
   b. OD width of weld plus buttering, as-built: 1.1 in. [8, Dimension D2+ D3]
3. Normal operating forces and moments due to deadweight and normal thermal expansion are listed in Table 1. These values are listed in the design basis fatigue analysis for the HPI nozzles [9, Page L-5 and L-7].
4. The operating pressure, P, is 2200 psig [9, pg. A-36].
5. The average operating temperature of the ANO-1 RCS cold leg piping is: 556°F [6.b].
6. The operating axial stress profiles (including weld residual stress) are defined in C-4728-00-01 R0 [3]. That analysis includes a partial-arc weld repair from the OD with 70% through-wall depth and with 90° included arc extent, centered at the 0° azimuth (Assumption 14):
   a. Case A: Weld centerline axial position at repair center (0° azimuthal position)
   b. Case B: Weld centerline axial position, averaged over partial-arc weld repair (5°-40° azimuthal position)
   c. Case C: Weld centerline axial position beyond edge of weld repair (55° azimuthal position)

d. Case D: Weld centerline axial position opposite weld repair center (180° azimuthal position)

e. Case E: Butter/DMW interface at repair center (0° azimuthal position)

f. Case F: Butter/DMW interface, averaged over partial-arc weld repair (5°-40° azimuthal position)

g. Case G: Butter/DMW interface beyond edge of weld repair (55° azimuthal position)

h. Case H: Butter/DMW interface opposite weld repair center (180° azimuthal position)

7. The materials of construction are as follows:

   a. The nozzle buttering and dissimilar metal weld are fabricated from Inconel weld material (Alloy 82/182) ([7.a, pg. 63] and [10, Item 25 of Table 3]).

   b. The safe end material is SA-479 Type 316 austenitic stainless steel [6.d, Part No. 133].

   c. The inlet nozzle is A-105 Grade II carbon steel [6.d, Part No. 46].

8. The crack growth rates for Alloy 182 are evaluated per the MRP-115 [11] crack growth rate disposition curve, which is also specified in Nonmandatory Appendix C of ASME Section XI [12].

9. Influence coefficients used in the stress intensity factor calculation were obtained from API 579-1 / ASME FFS-1 [13, Table 9B.14].

10. The allowable flaw size at the end of the evaluation period is determined in C-4728-00-02, Rev. 0 [4]. The results of that calculation indicate that the maximum allowable depth of 75% through-wall is applicable to circumferential flaws with a length up to 45% of the inner circumference.

4 ASSUMPTIONS

The following assumptions were applied in support of this calculation:

1. In accordance with the standard approach of the Nonmandatory Appendices A and C of ASME Section XI ([12] and [14]), circumferential surface flaws evaluated in this subcritical growth calculation are modeled to have a semi-elliptical shape. The maximum length of the modeled flaws remains much less than (< 50%) the inner circumference of the DMW, so transition to a full-circumference type flaw is not relevant.

2. The weld material is reported in technical documentation as Alloy 182 or Alloy 82 (Input 7.a). The standard deterministic crack growth rate for Alloy 182 per MRP-115 [11] and Nonmandatory Appendix C of ASME Section XI [12] is conservatively applied for the weld material as it is higher than the corresponding crack growth rate for Alloy 82 per these standard references.

3. The minimum wall thickness as reported during an ultrasonic examination (0.68 in., Input 2.a) is less than the nominal value (0.72 in., Input 1). Conservatively, this minimum as-built wall thickness is applied along with the nominal OD to define the geometry for the crack growth calculation.
4. An initial flaw depth of 10% through-wall ($a/t = 0.1$) is applied on the basis that this is the minimum flaw depth covered by the ASME Section XI Mandatory Appendix VIII, Supplement 10 qualifications for UT flaw detection [15].
5. As cracking degradation in Alloy 82/182 dissimilar metal piping butt welds is dominated by PWSCC, fatigue crack growth is not modeled in this calculation. Accordingly, the effects of transient loading are not considered to be significant and are thus not modeled.
6. An initial aspect ratio ($2c/a$) of 10 is conservatively applied, as longer flaws tend to have higher stress intensity factors at the deepest point. The aspect ratio is permitted to change due to differing growth rates at the surface tips and deepest point of the crack.
7. When calculating the effective bending moment and OD bending stress, circumferential cracks are conservatively assumed to be centered at the point of maximum bending tensile stress.
8. As the crack grows in length, the residual stress profile at the crack center is assumed to apply to the crack surface tips. C-4728-00-01, R0 [3] results indicate lower ID stresses are present beyond the repair region, so this assumption conservatively results in longer cracks.
9. Each component (M_x, M_y, and M_z) of the effective bending moment is calculated conservatively using the sum of the absolute value of the moment contributions (NTE, DW) for the same moment component, as in Equation [4-1]. The effective bending moment (M_{eff}) is then determined as a combination of the bending and torsional moments based on a von Mises stress approach:

$$M_i = \sum_j |M_{i,j}| \quad i = x, y, z \quad j = NTE, DW \qquad [4\text{-}1]$$

$$M_{\text{eff}} = \sqrt{M_y^2 + M_z^2 + \left(\frac{\sqrt{3}}{2} M_x\right)^2} \qquad [4\text{-}2]$$

10. Values for G_0 and G_1 influence coefficients are obtained by interpolating or extrapolating from tables in API Standard 579-1/ASME FFS-1 [13, Table 9B.14]. For input parameters outside the domains provided in the tables, extrapolation is performed as described by Assumption 11. For input parameters inside those domains, influence coefficients are determined through log-linear interpolation on t/R_i and on a/c, and linear interpolation on a/t.

11. Solutions for influence coefficients G_0 and G_1 are provided in API Standard 579-1/ASME FFS-1 [13] only for $a/t \leq 0.8$ and for $a/c \geq 0.125$ (for the t/R_i values of interest).

    a. In order to predict the time to through-wall growth, the influence coefficients are linearly extrapolated for the range $0.8 < a/t < 1.0$. Extrapolation of influence coefficients for $a/t > 0.8$ is considered to be standard practice, and has also been applied in probabilistic fracture mechanics codes such as xLPR (Extremely Low Probability of Rupture) [16]. Furthermore, the time required for a crack to grow from 10% through-wall to through-wall (which is affected by this extrapolation for $a/t > 0.8$) is considered to be a secondary result of this calculation. The time required for a crack to grow from 10% through-wall to the allowable depth (no greater than 75% through-wall), which is the primary result of this calculation, remains unaffected by this assumption.

    b. The influence coefficients are log-linearly extrapolated for $a/c < 0.125$ because there are no influence coefficients available in this range in API Standard 579-1/ASME FFS-1 for the t/R_i values of interest. It would be nonconservative to apply influence coefficients for $a/c = 0.125$ when calculating stress intensity factors for $a/c < 0.125$. Additionally, some influence coefficients for $a/c < 0.5$ are undefined because their lookup position would result in a flaw larger than the full circumference for the combination of a/t and t/R_i of interest, so these are log-linearly extrapolated in the same manner.

12. A plant capacity factor of 0.97 is applied to account for time in which the plant is not operating (e.g., due to refueling outages). This assumption is conservative since it corresponds to no operation for about 16 days out of a 1.5 year cycle.

13. The residual stress profile is represented as a piecewise linear stress profile, as defined within C-4728-00-01 R0 [3]. Defining a piecewise linear stress profile with a relatively fine spatial resolution of 2.5% through-wall (TW) as done here is considered appropriate for stresses output from finite-element analyses at discrete locations through the thickness of the weld ([14] and [17]).

14. The operating stress profile applied in the stress intensity factor calculations includes the weld residual stresses from a 90° partial-arc 70% through-wall localized weld repair performed from the outside diameter (OD), as calculated in C-4728-00-01, Rev. 0 [3]. This conservative weld repair assumption was developed on the basis of a review of fabrication records for the original dissimilar metal weld and the dissimilar metal weld performed during replacement of the safe end in 1982 ([7.a] and [1]). The modeling approach recommended in MRP-287 [5] includes consideration of weld repairs, even if no documented repairs have been identified—as is the case for this weld ([1, pg. S-2] and [18]). Given the length of the safe end (5.125 inches), the relatively small inside diameter at the subject weld (2.063 inches) makes weld repair from the inside of the weld infeasible. The use of a backing ring to make the weld joint demonstrates that all welding was performed from the outer surface of the joint. Hence, the 90° partial-arc repair extending about 70% of the distance from the outer surface was developed as a conservative weld repair assumption, with the worst-case stress profile from the three-dimensional WRS modeling applied in the crack growth evaluation. A partial arc repair type generates tensile residual stresses at the ID that are consistent with a hypothetical crack initiation at the ID surface. This conservative

approach was applied in lieu of the assumption of a 50% through-wall ID repair recommended in MRP-287 [5] because of the infeasibility of ID repair in this specific case.

15. A time step of 1 month is applied for the crack growth calculation. This time step is appropriately refined to yield converged results given the time-scale over which a crack grows through the thickness of the weld (i.e., greater than 15 years).

5 ANALYSIS

The purpose of this section is to describe the stress intensity factor calculations (Section 5.1) and crack growth calculations (Section 5.2) performed for the ANO-1 high pressure injection nozzle D Alloy 82/182 dissimilar metal piping butt weld. Deterministic crack growth calculations that are documented in this section are used to determine the time required for a circumferential crack to grow from an initial depth of 10% through-wall to a final depth of 75% through-wall (maximum allowable depth when flaw stability and length is not limiting ([4] and [12])).

5.1 Stress Intensity Factor Calculation

5.1.1 Loads and Stresses

Tensile stresses are one of the key factors influencing PWSCC. For the purposes of crack growth calculations, only stresses orthogonal to the plane of crack growth are considered (i.e. only stresses in the axial direction drive circumferential crack growth).

This calculation appropriately considers weld residual stresses, operating pressure stresses, operating temperature stresses, and piping loads due to dead weight and thermal expansion. The effect of transient stresses is not significant, as discussed in Assumption 5.

Weld residual stresses, operating pressure stresses, and operating temperature stresses were calculated using finite-element analyses that are documented in C-4728-00-01 [3]. The through-wall operating stress profile considering these load sources was determined in C-4728-00-01 [3] and is shown in Figure 3 (at the weld centerline) and Figure 4 (at the weld/butter interface). The axial position of these two profiles is shown schematically in Figure 2. The axial operating stress profile is given as $\sigma_{op,a}(x/t)$. The axial membrane stress due to the end cap pressure loading is included in the axial operating stress profile $\sigma_{op,a}(x/t)$ from the finite-element analysis.

Piping loads due to dead weight and normal thermal expansion act to create a longitudinal force component, a torsion moment, and two orthogonal bending moments. The axial membrane stresses due to dead weight and normal thermal expansion are calculated as follows:

$$\sigma_{\mathrm{DW},a} = \frac{F_{\mathrm{DW},x}}{A} \qquad [5\text{-}1]$$

$$\sigma_{\mathrm{NTE},a} = \frac{F_{\mathrm{NTE},x}}{A} \qquad [5\text{-}2]$$

Where:

$F_{\mathrm{DW},x}$ = the axial force due to dead weight
$F_{\mathrm{NTE},x}$ = the axial force due to normal thermal expansion
A = the axial cross-sectional area of the weld

A membrane stress accounting for the effect of crack face pressure, P, equal to the operating pressure acting on the crack face is also considered.

The axial bending stress is calculated using the bending moment and torsion components of the dead weight and normal thermal expansion piping loads. An effective bending moment (M_{eff}) is determined as a combination of the bending and torsional moments based on a von Mises stress approach, as discussed in Assumption 9:

$$M_{\mathrm{eff}} = \sqrt{M_y^2 + M_z^2 + \left(\frac{\sqrt{3}}{2} M_x\right)^2} \qquad [5\text{-}3]$$

Based on the moments specified in Table 1, an effective bending moment of 14.26 in-kips (1.611 kN-m) is calculated. The outer diameter (OD) bending stress at the point of maximum bending is then calculated as:

$$\sigma_B = \frac{M_{\text{eff}} R_o}{I} \quad [5\text{-}4]$$

$$I = \frac{\pi(R_o^4 - R_i^4)}{4} \quad [5\text{-}5]$$

where R_o is the weld outer radius and I is the moment of inertia of the weld cross-sectional area.

As the principle of superposition applies for linear-elastic fracture mechanics, the individual membrane stress contributions defined above are superimposed to obtain a total stress profile. The resulting total axial stress profile is defined as:

$$\sigma_{\text{tot},a}(x) = \sigma_{\text{op},a}(x) + \sigma_{\text{DW},a} + \sigma_{\text{NTE},a} + P \quad [5\text{-}6]$$

For circumferential cracks, the global bending stress, σ_B, is applied separately in the K_I calculation.

5.1.2 Universal Weight Function Method

Given the total axial stress profiles defined in Section 5.1.1, along with the depth and aspect ratio of the crack, stress intensity factors can be calculated. To facilitate flexibility in total stress profile applied to the crack face, instead of fitting a polynomial to the stress profile and applying the influence coefficient method, the universal weight function method is applied.

For circumferential cracks, the general form of the mode I stress intensity factor calculation by way of the universal weight function method, including the contribution to the mode I stress intensity factor due to a global bending moment, is given by [13]:

$$K_I = \sigma_B G_5 \sqrt{\frac{\pi a}{Q}} + \int_0^a h(x,a)\sigma_{\text{tot},a}(x)dx \quad [5\text{-}7]$$

where:

K_I = mode I stress intensity factor (MPa√m)

x = distance from the ID surface (m)

a = crack depth (m), and

$h(x,a)$ = weight function.

G_5 = influence coefficient for the effect of global bending on a circumferential flaw centered at the point of maximum bending stress

Q = flaw shape parameter defined below in Equation [5-16]

In general, the weight function, $h(x,a)$ is a function of the influence coefficients, G_0 and G_1. For the purpose of modeling crack growth under the semi-elliptical crack shape approximation (Assumption 1), the universal weight function method is applied to calculate separate stress intensity factors for the deepest point and the surface point of the semi-elliptical flaw.

For the deepest point, the influence coefficients G_0 and G_1 are determined as:

$$G_{90,i} = \sum_{n=0}^{6} A_{n,i} \qquad [5\text{-}8]$$

and for the surface point, the influence coefficients G_0 and G_1 are determined as:

$$G_{0,i} = A_{0,i} \qquad [5\text{-}9]$$

The individual $A_{n,i}$ fitting coefficients (including $A_{0,i}$) are obtained from linear-elastic finite element analyses. These fitting coefficients for semi-elliptical circumferential surface cracks on the ID surface are tabulated in API 579-1 / ASME FFS-1 [13, Table 9B.14] for specific combinations of the ratio of the weld thickness to inner radius (t/R_i), the ratio of the crack depth to crack half-length (a/c), and the ratio of the crack depth to the weld thickness (a/t).

Values from tables of G_0 and G_1 influence coefficients are interpolated in t/R_i, a/c, and a/t to obtain values of G_0 and G_1 specific to the crack geometry at a given timestep. This is accomplished by performing interpolation of the influence coefficients (Assumption 10):

1. Log-linear interpolation in t/R_i (i.e. linear interpolation of values on the scale $\ln(t/R_i)$)
2. Log-linear interpolation in a/c
   a. If $a/c < 0.125$, log-linearly extrapolate in a/c (Assumption 11)
   b. If $a/c < 0.5$ and interpolant value is undefined, log-linearly extrapolate in a/c (Assumption 11)
3. Linear interpolation in a/t
   a. If $a/t > 0.8$, linearly extrapolate up to $a/t = 1.0$ (Assumption 11).

Crack-geometry-specific G_0 and G_1 influence coefficients are then applied to compute the weight function coefficients, M_i (for the deepest point, 90°) and N_i (for the surface point, 0°) [13, Section 9B.5.15, 9B.14.2]:

$$M_1 = \frac{2\pi}{\sqrt{2Q}}\left(3G_{90,1} - G_{90,0}\right) - \frac{24}{5} \quad [5\text{-}10]$$

$$M_2 = 3 \quad [5\text{-}11]$$

$$M_3 = \frac{6\pi}{\sqrt{2Q}}\left(G_{90,0} - 2G_{90,1}\right) + \frac{8}{5} \quad [5\text{-}12]$$

$$N_1 = \frac{3\pi}{\sqrt{Q}}\left(2G_{0,0} - 5G_{0,1}\right) - 8 \quad [5\text{-}13]$$

$$N_2 = \frac{15\pi}{\sqrt{Q}}\left(3G_{0,1} - G_{0,0}\right) + 15 \quad [5\text{-}14]$$

$$N_3 = \frac{3\pi}{\sqrt{Q}}\left(3G_{0,0} - 10G_{0,1}\right) - 8 \qquad [5\text{-}15]$$

where the flaw shape parameter, Q, is applied using the definition in API 579-1 / ASME FFS-1 [13, Section 9B.3.4.1]:

$$Q = \begin{cases} 1.0 + 1.464\left(\frac{a}{c}\right)^{1.65} & \text{for a/c} \le 1.0 \\ 1.0 + 1.464\left(\frac{c}{a}\right)^{1.65} & \text{for a/c} > 1.0 \end{cases} \qquad [5\text{-}16]$$

For the deepest point of a semi-elliptical surface crack, the weight function, h_{90}, is then defined as [13, Section 9B.14.1]:

$$h_{90}(x,a) = \frac{2}{\sqrt{2\pi(a-x)}}\left[1 + M_1\left(1-\frac{x}{a}\right)^{1/2} + M_2\left(1-\frac{x}{a}\right) + M_3\left(1-\frac{x}{a}\right)^{3/2}\right] \qquad [5\text{-}17]$$

Similarly, for the surface point of the crack, the weight function, h_0, is defined as [13, Section 9B.14.1]:

$$h_0(x,a) = \frac{2}{\sqrt{\pi x}}\left[1 + N_1\left(\frac{x}{a}\right)^{1/2} + N_2\left(\frac{x}{a}\right) + N_3\left(\frac{x}{a}\right)^{3/2}\right] \qquad [5\text{-}18]$$

The integrals for the stress intensity factors are evaluated using a closed-form solution that leverages the piecewise linear nature of the stress profile, as described in Section 5.1.2.1. These expressions for the stress intensity factors are evaluated at each time step as an input to the crack growth calculation, which is detailed in Section 5.2.

5.1.2.1 Weight Function Integral Equations

An integration approach was applied that uses closed-form expressions for the weight function integrals [17]. In effect, Equations [5-22] and [5-27] in this subsection are implemented in the code instead of performing numeric integration using Equations [5-7], [5-17], and [5-18].

The closed-form expressions leverage the b_i and k_i piecewise linear parameters defined in Equations [5-20] and [5-21], respectively. For example, the total operating stress profiles from C-4728-00-01 R0 [3] is effectively applied as a series of linear equations defined in increments of 2.5% through-wall (Assumption 13). The i^{th} linear segment of the discrete total stress profile with a total of n segments (n+1 points) can be defined using the following notation ([14, A-3221] and [17]):

$$\sigma_{tot,i}(x) = k_i x + b_i \qquad [5\text{-}19]$$

where

$$b_i = \sigma_{tot}(x_i) - x_i\left(\frac{\sigma_{tot}(x_{i+1}) - \sigma_{tot}(x_i)}{x_{i+1} - x_i}\right) \qquad [5\text{-}20]$$

$$k_i = \frac{\sigma_{tot}(x_{i+1}) - \sigma_{tot}(x_i)}{x_{i+1} - x_i} \qquad [5\text{-}21]$$

and

$\sigma_{tot}(x_i)$ = discrete data points for total stress profile
$\sigma_{tot,i}(x)$ = piece-wise linear representation of total stress profile
x_i = locations of discrete data points at which the total stress profile, $\sigma_{tot}(x_i)$, is defined.

In the closed-form expressions for the stress intensity factor, crack-geometry-specific influence coefficients G_0 and G_1 are applied to compute the weight function coefficients, M_i (for the deepest point) and N_i (for the surface point) defined in Equations [5-10] through [5-15].

The closed-form solution for stress intensity factor at the deepest point of a circumferential crack is ([14, A-3421] and [17]):

$$K_{I,90}(k_i, b_i) = \sigma_B G_{5,90}\sqrt{\frac{\pi a}{Q}} + K_{IM0} + K_{IM1}M_1 + K_{IM2}M_2 + K_{IM3}M_3 \quad [5\text{-}22]$$

where

$$K_{IM0} = \frac{2\sqrt{2}}{3\sqrt{\pi}}\sum_{i=1}^{n}\left[(k_i x_i + 2k_i a + 3b_i)\sqrt{a - x_i} - (k_i x_{i+1} + 2k_i a + 3b_i)\sqrt{a - x_{i+1}}\right] \quad [5\text{-}23]$$

$$K_{IM1} = \frac{\sqrt{2}}{\sqrt{\pi a}}\sum_{i=1}^{n}\left[\frac{k_i}{2}(x_{i+1}^2 - x_i^2) + b_i(x_{i+1} - x_i)\right] \quad [5\text{-}24]$$

$$K_{IM2} = \frac{2}{15a}\frac{\sqrt{2}}{\sqrt{\pi}}\sum_{i=1}^{n}\left[(3k_i x_i + 2k_i a + 5b_i)(a - x_i)^{3/2} - (3k_i x_{i+1} + 2k_i a + 5b_i)(a - x_{i+1})^{3/2}\right] \quad [5\text{-}25]$$

$$K_{IM3} = \sqrt{\frac{2}{\pi}}\frac{1}{a\sqrt{a}}\sum_{i=1}^{n}\left[\frac{k_i}{3}(x_i^3 - x_{i+1}^3) + \frac{1}{2}(k_i a - b_i)x_{i+1}^2 - \frac{1}{2}(k_i a - b_i)x_i^2 + b_i a(x_{i+1} - x_i)\right] \quad [5\text{-}26]$$

Similarly, the closed-form solution for the stress intensity factor at the surface point of a circumferential crack is ([14, A-3421] and [17]):

$$K_{I,0}(k_i, b_i) = \sigma_B G_{5,0} \sqrt{\frac{\pi a}{Q}} + K_{IN0} + K_{IN1} N_1 + K_{IN2} N_2 + K_{IN3} N_3 \quad [5\text{-}27]$$

where

$$K_{IN0} = \frac{4}{3\sqrt{\pi}} \sum_{i=1}^{n} \left[\sqrt{x_{i+1}} (k_i x_{i+1} + 3b_i) - \sqrt{x_i} (k_i x_i + 3b_i) \right] \quad [5\text{-}28]$$

$$K_{IN1} = \frac{1}{\sqrt{\pi a}} \sum_{i=1}^{n} \left[x_{i+1} (k_i x_{i+1} + 2b_i) - x_i (k_i x_i + 2b_i) \right] \quad [5\text{-}29]$$

$$K_{IN2} = \frac{4}{15a\sqrt{\pi}} \sum_{i=1}^{n} \left[x_{i+1}^{3/2} (3k_i x_{i+1} + 5b_i) - x_i^{3/2} (3k_i x_i + 5b_i) \right] \quad [5\text{-}30]$$

$$K_{IN3} = \frac{1}{3a\sqrt{\pi a}} \sum_{i=1}^{n} \left[x_{i+1}^2 (2k_i x_{i+1} + 3b_i) - x_i^2 (2k_i x_i + 3b_i) \right] \quad [5\text{-}31]$$

5.2 Crack Growth Calculation

5.2.1 Approach

The crack growth rates for circumferential cracks in the Alloy 82/182 weld metal are calculated considering the PWSCC growth mechanism. Per Assumption 5, as cracking degradation in the subject weld is dominated by PWSCC, fatigue crack growth is not modeled in this calculation. Accordingly,

the standard PWSCC crack growth rate equation for Alloy 182 ([11] and [12]) is applied for the crack growth calculation (see Assumption 2):

$$\frac{da}{dt} = \exp\left[-\frac{Q_g}{R}\left(\frac{1}{T}-\frac{1}{T_{ref}}\right)\right]\alpha K_{I,90}^{\beta} \quad [5\text{-}32]$$

$$\frac{dc}{dt} = \exp\left[-\frac{Q_g}{R}\left(\frac{1}{T}-\frac{1}{T_{ref}}\right)\right]\alpha K_{I,0}^{\beta} \quad [5\text{-}33]$$

where

da/dt = crack growth rate at the deepest point of the crack (m/s)
dc/dt = crack growth rate at the surface point of the crack (m/s)
Q_g = thermal activation energy for crack growth = 130 kJ/mol ([11] and [12])
R = universal gas constant = 8.314×10^{-3} kJ/mol-K
T = absolute operating temperature at crack location = 564.26 K (Input 5)
T_{ref} = absolute temperature (325°C) used to normalize crack growth data = 598.15 K ([11] and [12])
α = crack growth rate coefficient for Alloy 182 = 1.5×10^{-12} at 325°C for m/s and MPa·m$^{0.5}$ ([11] and [12])
$K_{I,90}$ = stress intensity factor at the deepest point of the crack, calculated per Section 5.1 (MPa·m$^{0.5}$)
$K_{I,0}$ = stress intensity factor at the surface point of the crack, calculated per Section 5.1 (MPa·m$^{0.5}$)
β = crack growth rate exponent = 1.6 ([11] and [12])

To model growth of the cracks over time, the crack growth rate is calculated and integrated to determine the new crack length and depth using one-month time steps (Assumption 15). The crack growth rates obtained in Equations [5-32] and [5-33] are multiplied by the plant capacity factor (Assumption 12) to account for calendar time in which the plant is not operating (e.g., due to refueling outages). Using this approach, the times required (1) to produce a flaw with a depth of 75% through-

wall (maximum allowable depth when flaw stability is not limiting) and (2) for the flaw to penetrate through-wall (resulting in leakage) are calculated.

Initial conditions applied assume an initial depth of 10% through-wall (Assumption 4), along with an initial aspect ratio ($2c/a$) of 10 (Assumption 6). The full set of operating stress profiles from Input 6 were evaluated, assuming a 90° partial-arc weld repair with a 70% through-wall depth performed from the OD surface (Assumption 14).

5.2.2 Results

The times required for a flaw with an initial depth of 10% through-wall to grow (1) to a depth of 75% through-wall (maximum allowable depth per ASME Section XI when flaw stability is not limiting [4]) and (2) through-wall are reported in Table 2. There are three stress cases of primary interest:

- The case with limiting crack growth in depth, Case B (weld centerline axial position, averaged over partial-arc weld repair (5°-40° azimuthal position))
- The case with limiting crack growth in length, Case E (DMW/butter interface axial position, at the repair center (0° azimuthal position))
- A case with minimal influence from the weld repair, Case D (weld centerline axial position, opposite/180° from weld repair center)

The results for the three stress cases of primary interest are shown in Figure 5 through Figure 10. Crack depth as a function of time is shown in Figure 5, Figure 6 shows the crack total length on the ID surface ($2c/\pi D_i$) as a function of time, and Figure 7 shows the crack aspect ratio ($2c/a$) as a function of time. In addition, plots are provided showing the crack-tip stress intensity factors applied in the crack growth equation. Figure 8, Figure 9, and Figure 10 show the crack-tip stress intensity factor at the deepest point (K_{90}) and at the surface point (K_0) as a function of crack depth (a/t) for cases B, E, and D, respectively.

Allowable flaw size calculations in C-4728-00-02 [4], performed in accordance with ASME Section XI, result in an allowable depth of 75% through-wall for circumferential flaw lengths up to at least 45% of the circumference. For all the crack growth cases (A through H), the flaw depth and length remain within these allowable limits for well beyond 7.5 years. After 7.5 years of growth, Case B has a depth of about 35% through-wall and a length of about 15% of the inner circumference, and Case E has a depth of about 33% through-wall and a length of about 21% of the inner circumference.

For Case B (the limiting flaw depth case), the time for a flaw to grow from an initial depth of 10% through-wall to the allowable depth of 75% through-wall is 14.6 years, and an additional 1.2 years is calculated for the crack to penetrate through the remaining 25% of the wall thickness. For Case E (limiting flaw length case), the total flaw length on the ID ($2c/\pi D_i$) reaches 43% of the circumference by the time it grows to 75% through-wall after 20.2 years.

5.3 Software Usage

The following software, controlled in accordance with DEI's quality assurance program for nuclear safety-related work [19], was used in preparing this calculation.

The stress intensity factor and crack growth calculations used in this work were performed using Python 3.7 as a one-time-use engineering analysis computer program on a Dell Precision 5520 with an Intel Core i7-7820HQ processor and running Windows 10 Pro N (Build 19041). The results from this one-time-use program were checked and reviewed in accordance with DEI's nuclear quality assurance (QA) program manual [19]. Each output from the one-time-use Python calculation is individually verified in Memo M-4728-00-02 [20]. The alternate calculation documented in the memo was performed using Excel for Office 365. Native electronic files for the Software Usage Records associated with the above software use are included in the data disk that accompanies this calculation [21]. These files are listed in Appendix A of this calculation.

6 REFERENCES

1. Letter from L.M. Lesniak (AREVA) to K. Ehren (Entergy), "Transmittal of 1982 High Pressure Injection and Makeup Line Non-Destructive Examination Report, 58-1124606-00," dated September 25, 2008.
2. ASME Code Case N-770-5, "Alternative Examination Requirements and Acceptance Standards for Class 1 PWR Piping and Vessel Nozzle Butt Welds Fabricated With UNS N06082 or UNS W86182 Weld Filler Material With or Without Application of Listed Mitigation Activities," Section XI, Division 1, American Society of Mechanical Engineers, New York, Approval Date: November 7, 2016.
3. Dominion Engineering, Inc. Calculation C-4728-00-01, Revision 0, August 2020.
4. Dominion Engineering, Inc. Calculation C-4728-00-02, Revision 0, August 2020.
5. *Materials Reliability Program: Primary Water Stress Corrosion Cracking (PWSCC) Flaw Evaluation Guidance (MRP-287)*. EPRI, Palo Alto, CA: 2010. 1021023. [Freely available at www.epri.com]
6. Email from R. Nettles (Entergy) to K. Fuhr (DEI), "RE: Contract 10610028 – Inputs for ANO1 HPI "D" Nozzle Analysis," dated May 19, 2020. DEI Incoming Correspondence IC-4728-00-01, with attachments:
   a. "U1 Primary CEI Data Summary" from 8/1/2018 to 8/31/2019 (file: chemistry data.docx)
   b. Email from D. Barborek (Entergy) to R. Nettles (Entergy), "Cold Leg Temperature for "D" HPI Nozzle Relief Request," dated May 19, 2020. (file: Cold Leg Temperature for "D" HPI Nozzle Relief Request.msg)
   c. EC No.: 8901, "HPI Nozzle Drawing Impacts," EN-DC-115, Rev. 5. (file: EC-8901 Writeup.pdf)
   d. Arkansas Nuclear One, Unit 1, Engineering Change Markup Drawing, "List of Material, Coolant Piping," M1E-32, Rev. 2, Sheet 1, September 3, 2008. (file: M1E 32 EC-8901.pdf)
   e. Arkansas Nuclear One, Unit 1, Engineering Change Markup Drawing, "B-Thermal Sleeve," 65530-1, Rev. 0, Sheet 1, September 3, 2008. (file: 65530-1 SH1 EC-8901.pdf)
   f. Arkansas Nuclear One, Unit 1, Engineering Change Markup Drawing, "New Safe End," 65530-2, Rev. 0, Sheet 1, September 3, 2008. (file: 65530-2 sh1 EC-8901.pdf)
   g. Arkansas Nuclear One, Unit 1, Engineering Change Markup Drawing, "Assembly & Detail for 2 1/2" Pressure Injection Nozzle," M1E-14, Rev. NEW, Sheet 2, September 3, 2008. (file: M1E-14 SH2 EC-8901.pdf)

h. Arkansas Nuclear One, Unit 1, Engineering Change Markup Drawing, "Assembly & Detail for 2 1/2" Pressure Injection Nozzle," M1E-14, Rev. 5, Sheet 1, September 3, 2008. (file: M1E-14 EC 8901.pdf)

i. Arkansas Nuclear One, Unit 1, Engineering Change 0000008901, Rev. 0, "HPI Nozzle Drawing Impacts," Approved September 25, 2008. (file: ec-ano-0000008901-000.pdf)

7. Email from R. Nettles (Entergy) to K. Fuhr (DEI), "RE: Contract 10610028 – Inputs for ANO1 HPI "D" Nozzle Analysis," dated May 19, 2020. DEI Incoming Correspondence IC-4728-00-02, with attachment:

   a. "Design Change / Plant Change Closeout Form – DCP No. 82-1018 & ECN 1, 2, 3, 4, & 5," July 1982. (file: micro film 2007_001.pdf)

8. Dissimilar-Metal Weld Walk-Down Data Sheet 1, "2.5" HPI NOZZLE ON "D" UPPER COLD LEG – FLOW IS INTO THE COLD LEG," Report No.: BOP-UT-05-053, October 16, 2005.

9. E. Dietrich, "ASME Class 1 Fatigue Analysis for HPI/RCS Nozzles & Stress Report," 86-E-0074-57, Rev. 5, November 6, 1995.

10. D. Smith, Entergy Supplemental Form ER-ANO-2003-0245-027, Rev. 0, dated May 14, 2008.

11. *Materials Reliability Program Crack Growth Rates for Evaluating Primary Water Stress Corrosion Cracking (PWSCC) of Alloy 82, 182, and 132 Welds (MRP-115)*, EPRI, Palo Alto, CA: 2004. 1006696. [Freely available at www.epri.com]

12. ASME Boiler and Pressure Vessel Code, Section XI, Nonmandatory Appendix C. 2017 Edition.

13. API Standard 579-1/ASME FFS-1 Fitness for Service, 2016.

14. ASME Boiler and Pressure Vessel Code, Section XI, Nonmandatory Appendix A. 2017 Edition.

15. ASME Boiler and Pressure Vessel Code, Section XI, Mandatory Appendix VIII. 2017 Edition.

16. D. Rudland, D.-J. Shim, and S. Xu, "Simulating Natural Axial Crack Growth in Dissimilar Metal Welds due to Primary Water Stress Corrosion Cracking," *Proceedings of ASME 2013 Pressure Vessels and Piping Conference*, July 14-18, 2013, Paris, France, ASME, 2013. PVP2013-97188.

17. S. Xu, D. Lee, D. Scarth, and R. Cipolla, "Closed-Form Relations for Stress Intensity Factor Influence Coefficients for Axial ID Surface Flaws in Cylinders for Appendix A of ASME Section XI," *Proceedings of the ASME 2014 Pressure Vessels & Piping Conference*, July 20-24, 2014, Anaheim, California, USA, 2014. PVP2014-28222.

18. Radiographic Inspection Report, Weld Number: "Safe End to Nozzle," System Number: "HPI Line to Pump P32D," dated April 21, 1982.

19. Dominion Engineering, Inc., *Quality Assurance Manual for Safety-Related Nuclear Work*, DEI-002, Revision 18, November 2010.

20. Dominion Engineering, Inc. Memorandum M-4728-00-02, Revision 0, August 2020.

21. Dominion Engineering, Inc. Data Disk D-4728-00-02, Revision 0, August 2020.

22. Babcock & Wilcox Company, *Babcock & Wilcox 177 Fuel Assembly Owner's Group Safe End Task Force Report on Generic Investigation of HPI/MU Nozzle Component Cracking*, 77-1140611-00. [NRC ADAMS Accession No: ML15224A784]

Table 1. Inputs: Piping Loads and Moments at the DMW [9, pg. L-5 and L-7]

Variable	Units	Deadweight	Normal Thermal Expansion
F_x (axial force, + toward RCS piping)	lbf	11	173
M_x (torsional moment about nozzle centerline)	in-lbf	-393	-5045
M_y (moment about vertical axis)	in-lbf	-358	-1678
M_z (moment about transverse axis)	in-lbf	2296	-11013

Table 2. Crack Growth Results

Case	Stress Profile		Growth Time to 75% TW (yr)	Growth Time to TW (yr)
	Axial Position	Angular Position		
A	DMW Centerline	Repair Center	18.0	19.3
B	DMW Centerline	Average Over Repair	14.6	15.8
C	DMW Centerline	Beyond Repair	Growth Arrests	Growth Arrests
D	DMW Centerline	Opposite Repair	Depth Growth Arrests	Depth Growth Arrests
E	Butter/DMW Interface	Repair Center	20.1	21.1
F	Butter/DMW Interface	Average Over Repair	15.8	16.7
G	Butter/DMW Interface	Beyond Repair	Growth Arrests	Growth Arrests
H	Butter/DMW Interface	Opposite Repair	Depth Growth Arrests	Depth Growth Arrests

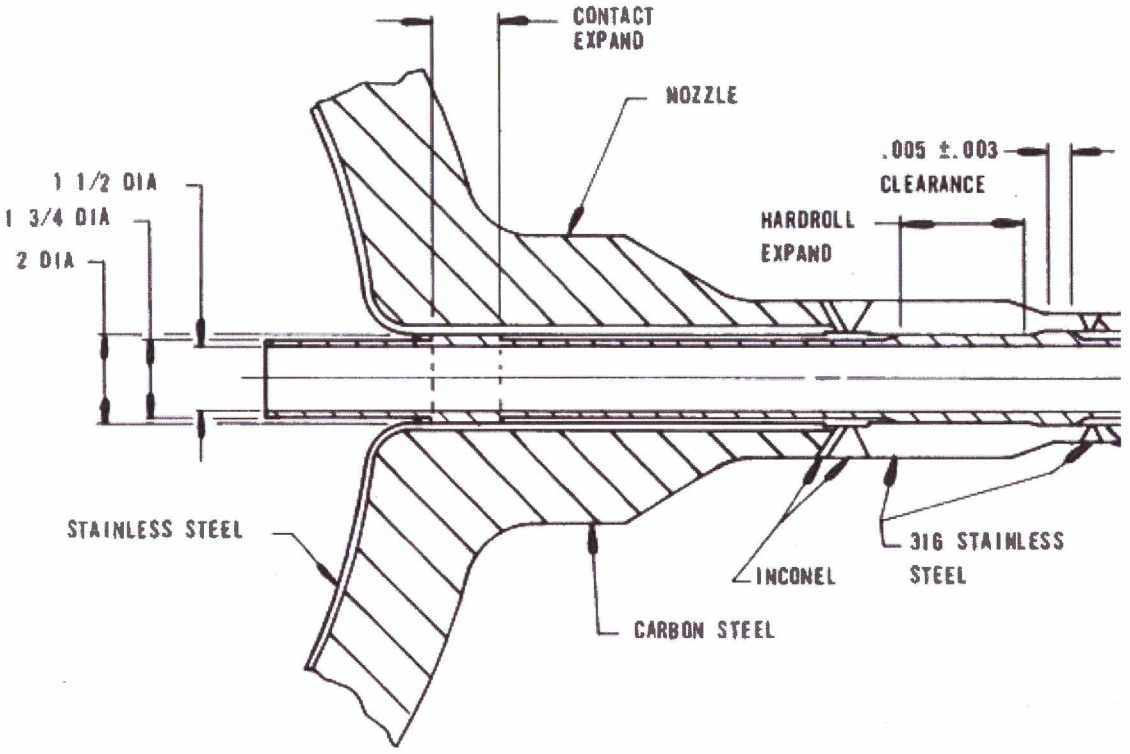

Figure 1. Configuration of HPI Nozzle in B&W Plant such as ANO-1 (From Reference [22])

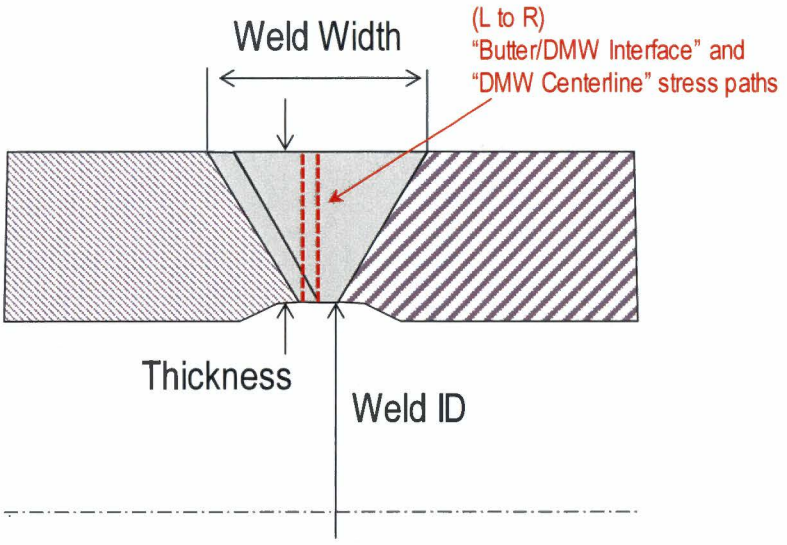

Figure 2. Key Dimensions for Single-V Weld Configuration

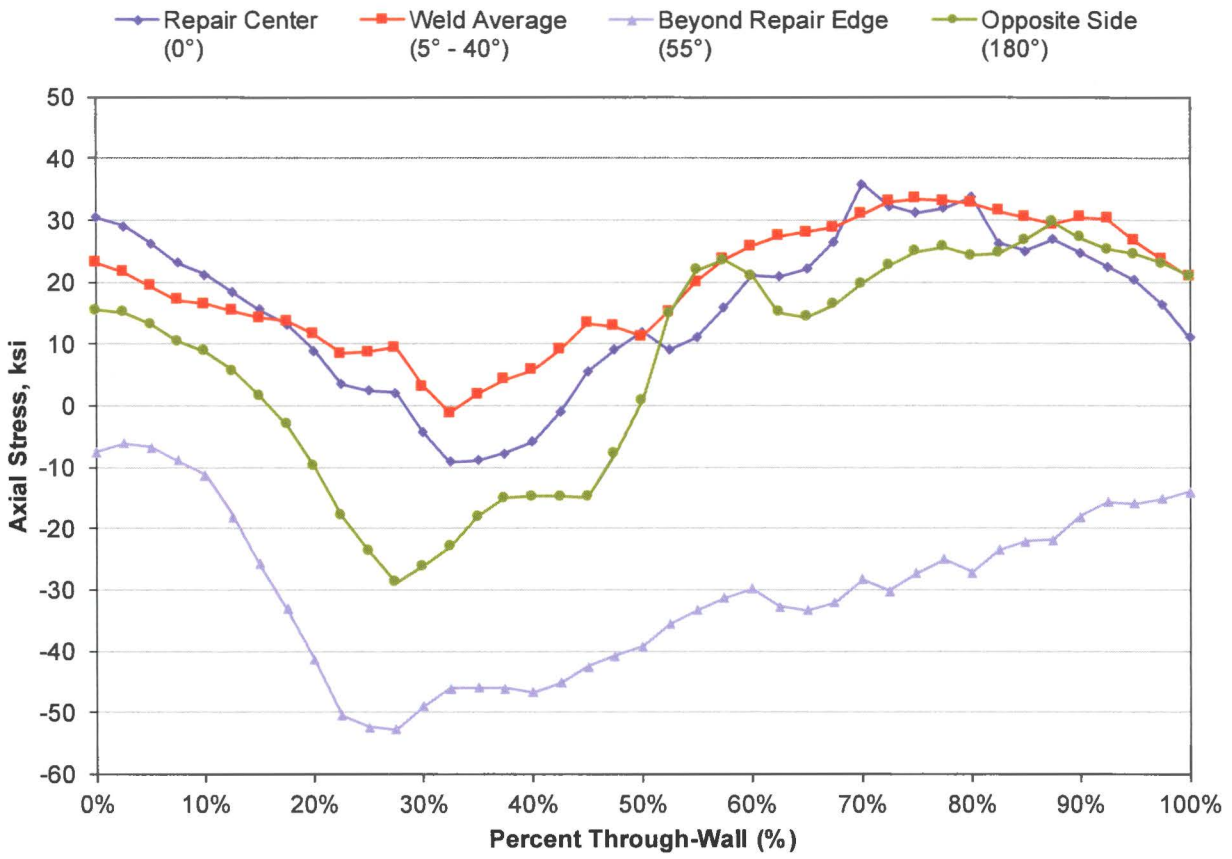

Figure 3. Residual Plus Operating Stress Profiles Applied for PWSCC Crack Growth Calculations at the DMW Centerline, Cases A-D (From Reference [3])

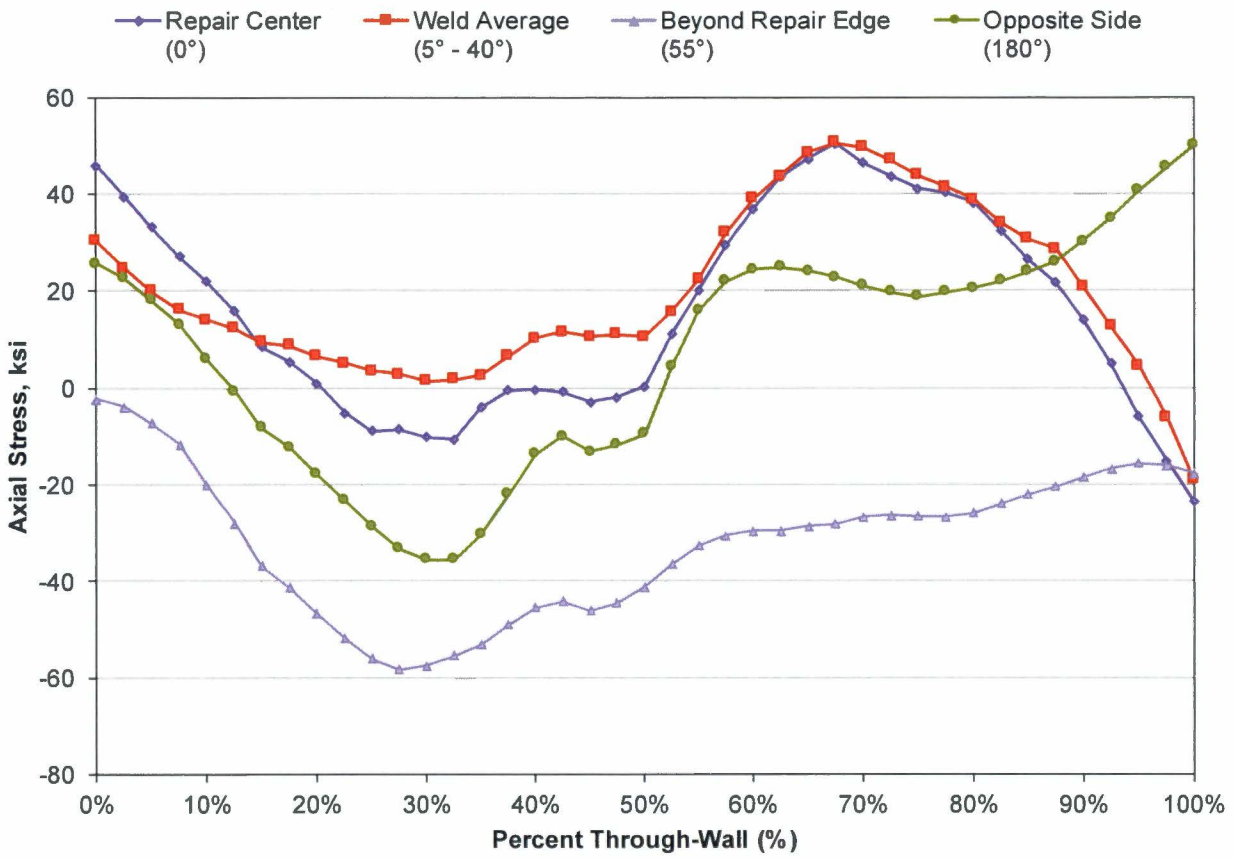

Figure 4. Residual Plus Operating Stress Profiles Applied for PWSCC Crack Growth Calculations at the Butter/DMW Interface, Cases E-H (From Reference [3])

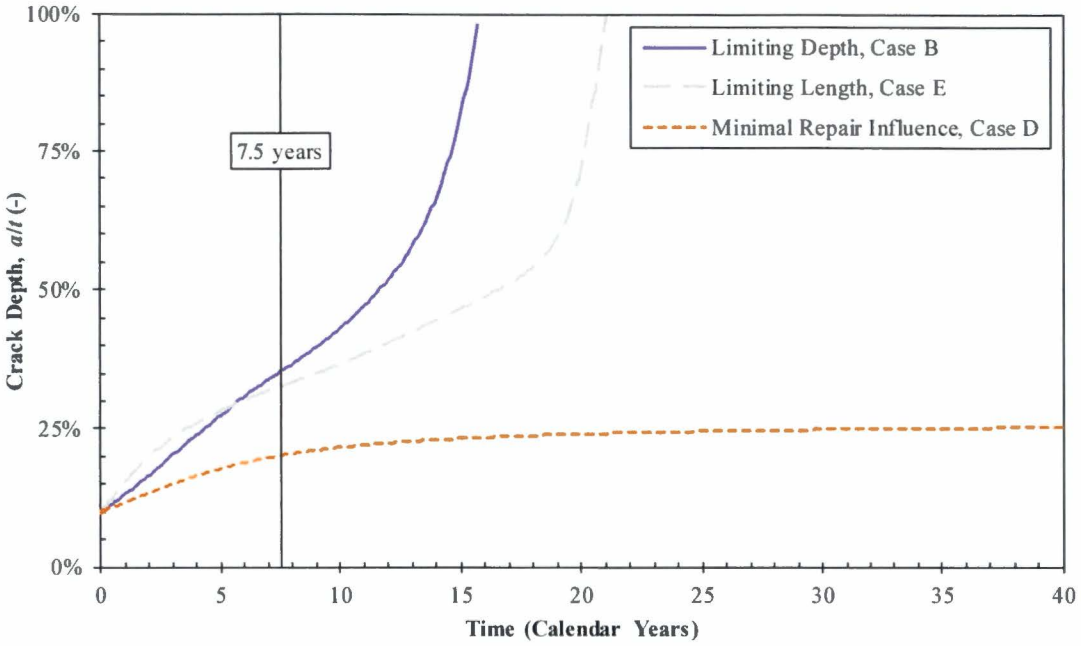

Figure 5. Crack Depth, *a/t*, as a Function of Time

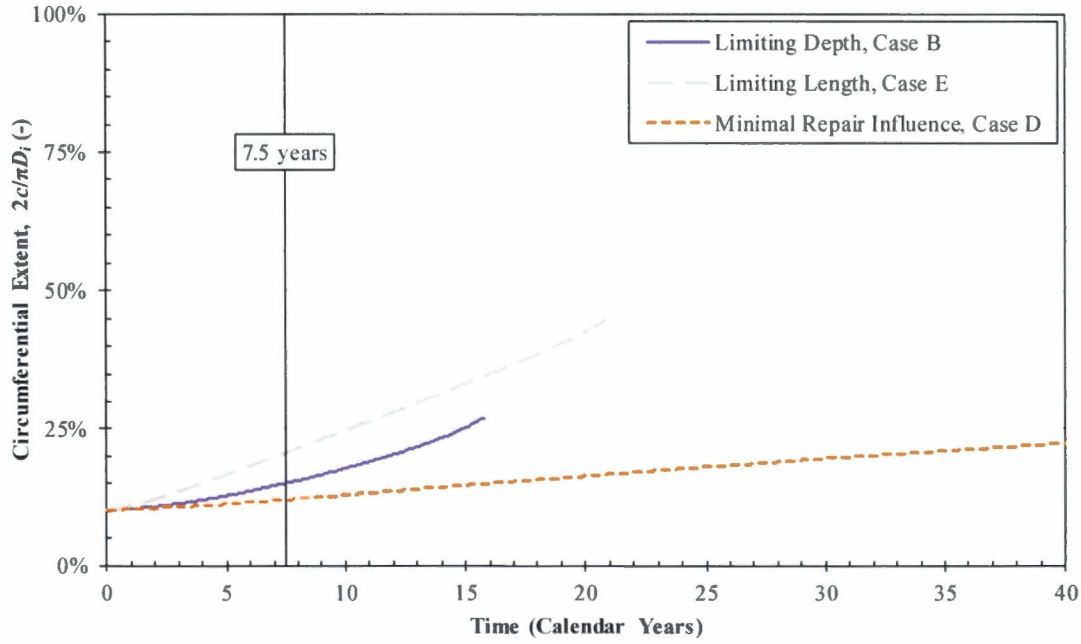

Figure 6. Crack Half-Length on ID, $2c/\pi D_i$, as a Function of Time

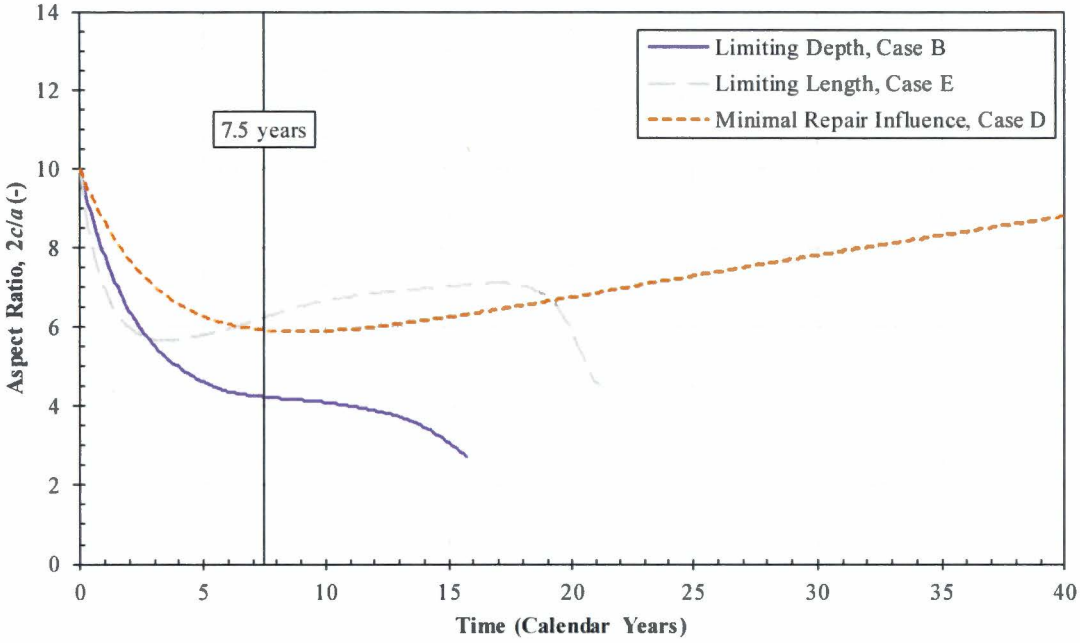

Figure 7. Crack Aspect Ratio, 2*c*/*a*, as a Function of Time

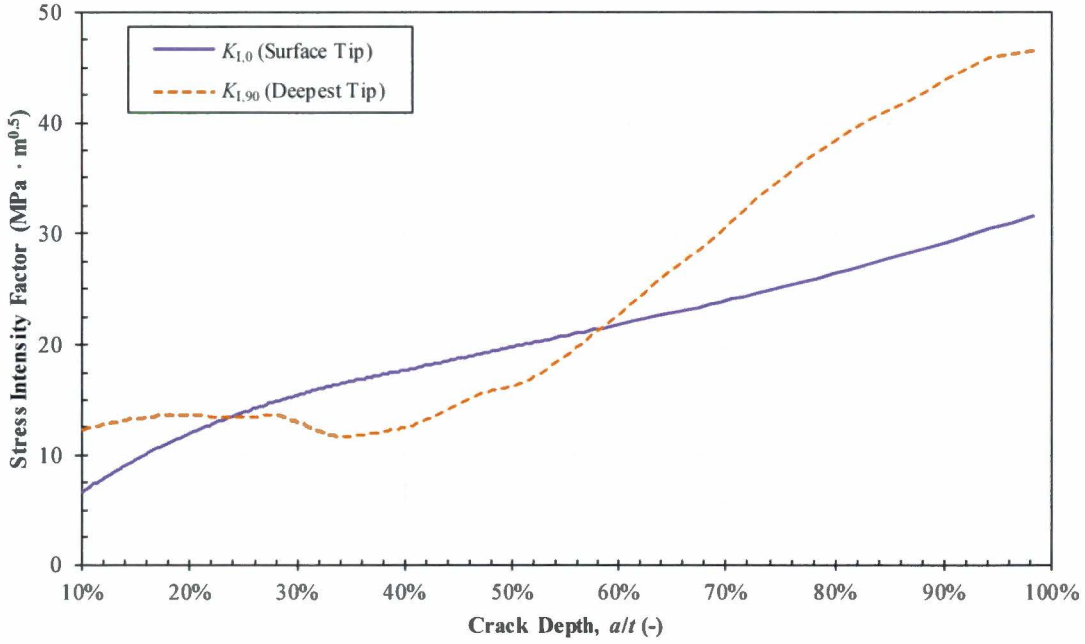

Figure 8. Crack Tip Stress Intensity Factor as a Function of Crack Depth for Limiting Case in Depth (Case B)

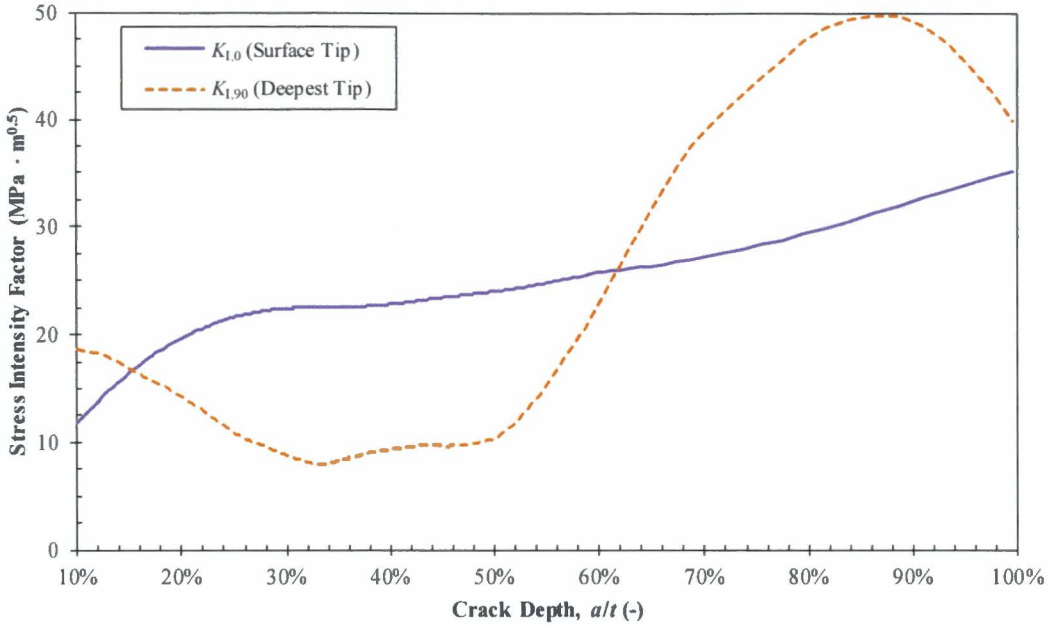

Figure 9. Crack Tip Stress Intensity Factor as a Function of Crack Depth for Limiting Case in Length (Case E)

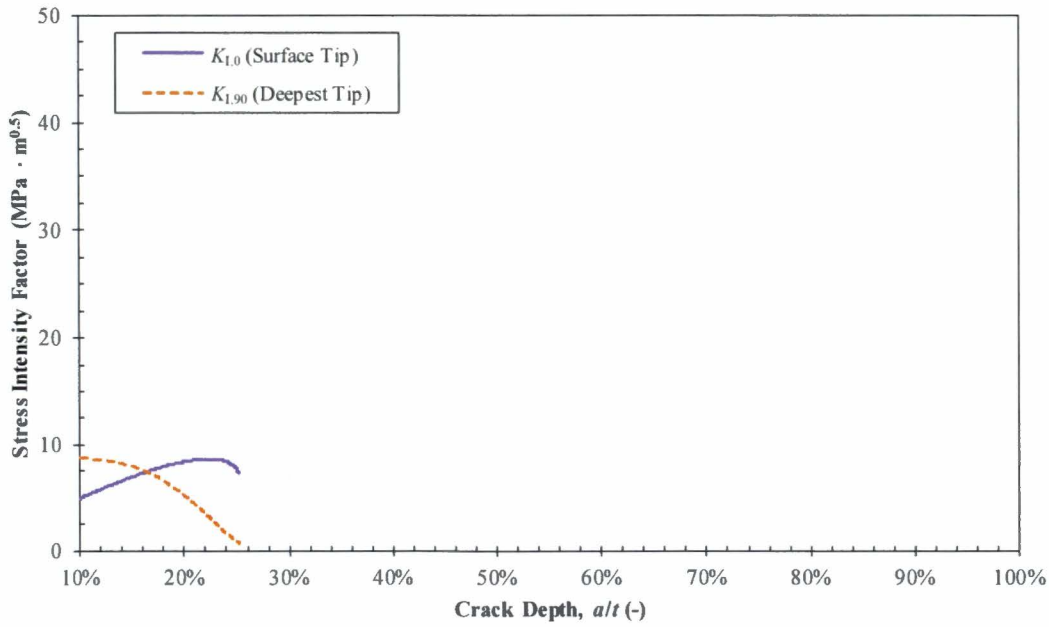

Figure 10. Crack Tip Stress Intensity Factor as a Function of Crack Depth for Case with Minimal Influence from the Weld Repair (Case D)

A CONTENTS OF DATA DISK D-4728-00-02 [21]

The following tables list the contents of Data Disk D-4728-00-02. The contents include Software Usage Records in their native electronic formats.

Table A-1. Software Usage Records

Software Usage Records		
Folder	**File name**	**Description**
A Weld_0	A-cen0.inp	Echo of the input file and stress listing for this case.
	A-cen0.yaml	Input listing for this case.
	A-cen0_gcoeffs.txt	Listing of WFM coefficients for this case (interpolated on t/R).
	A-cen0_out.png	Automatically generated plot of the results for this case.
	A-cen0_out.txt	Results file (crack parameters as function of time).
	HPI_cen_0_axial.csv	Axial operating stress profile from FEA (MPa).
B Weld_5-40	B-cen_weldavg.inp	Echo of the input file and stress listing for this case.
	B-cen_weldavg.yaml	Input listing for this case.
	B-cen_weldavg_gcoeffs.txt	Listing of WFM coefficients for this case (interpolated on t/R).
	B-cen_weldavg_out.png	Automatically generated plot of the results for this case.
	B-cen_weldavg_out.txt	Results file (crack parameters as function of time).
	HPI_cen_weldavg_axial.csv	Axial operating stress profile from FEA (MPa).
C Weld_55	C-cen55.inp	Echo of the input file and stress listing for this case.
	C-cen55.yaml	Input listing for this case.
	C-cen55_gcoeffs.txt	Listing of WFM coefficients for this case (interpolated on t/R).
	C-cen55_out.png	Automatically generated plot of the results for this case.
	C-cen55_out.txt	Results file (crack parameters as function of time).
	HPI_cen_55_axial.csv	Axial operating stress profile from FEA (MPa).
D Weld_180	D-cen180.inp	Echo of the input file and stress listing for this case.
	D-cen180.yaml	Input listing for this case.
	D-cen180_gcoeffs.txt	Listing of WFM coefficients for this case (interpolated on t/R).
	D-cen180_out.png	Automatically generated plot of the results for this case.
	D-cen180_out.txt	Results file (crack parameters as function of time).
	HPI_cen_180_axial.csv	Axial operating stress profile from FEA (MPa).
E Butter_0	E-btr0.inp	Echo of the input file and stress listing for this case.
	E-btr0.yaml	Input listing for this case.
	E-btr0_gcoeffs.txt	Listing of WFM coefficients for this case (interpolated on t/R).
	E-btr0_out.png	Automatically generated plot of the results for this case.
	E-btr0_out.txt	Results file (crack parameters as function of time).
	HPI_btr_0_axial.csv	Axial operating stress profile from FEA (MPa).

Table A-1. Software Usage Records (Continued)

Software Usage Records		
Folder	**File name**	**Description**
F Butter_5-40	F-btr_weldavg.inp	Echo of the input file and stress listing for this case.
	F-btr_weldavg.yaml	Input listing for this case.
	F-btr_weldavg_gcoeffs.txt	Listing of WFM coefficients for this case (interpolated on t/R).
	F-btr_weldavg_out.png	Automatically generated plot of the results for this case.
	F-btr_weldavg_out.txt	Results file (crack parameters as function of time).
	HPI_btr_weldavg_axial.csv	Axial operating stress profile from FEA (MPa).
G Butter_55	G-btr55.inp	Echo of the input file and stress listing for this case.
	G-btr55.yaml	Input listing for this case.
	G-btr55_gcoeffs.txt	Listing of WFM coefficients for this case (interpolated on t/R).
	G-btr55_out.png	Automatically generated plot of the results for this case.
	G-btr55_out.txt	Results file (crack parameters as function of time).
	HPI_btr_55_axial.csv	Axial operating stress profile from FEA (MPa).
H Butter_180	H-btr180.inp	Echo of the input file and stress listing for this case.
	H-btr180.yaml	Input listing for this case.
	H-btr180_gcoeffs.txt	Listing of WFM coefficients for this case (interpolated on t/R).
	H-btr180_out.png	Automatically generated plot of the results for this case.
	H-btr180_out.txt	Results file (crack parameters as function of time).
	HPI_btr_180_axial.csv	Axial operating stress profile from FEA (MPa).
Common Files	calc_K_wfm.py	Python script that creates the object for calculating stress intensity factor
	butt_weld_cracking_wfm.py	Python script that generates the output files
	requirements.txt	Listing of required Python packages and version number
	WFM-Table9B14_circ_id.csv	API 579-1/AMSE FFS-1 Table 9B.14 coefficient lookup table
Check Documents	M-4728-00-02 R0.pdf	Memo documenting alternate calculation for one-time use engineering analysis computer program.
	ANO1 HPI (A - Weld CL - Repair Center).xlsm	Alternate calculation for 0° case at the weld centerline
	ANO1 HPI (B - Weld CL - Avg Over Repair).xlsm	Alternate calculation for case averaged over the repair length at the weld centerline
	ANO1 HPI (C - Weld CL - Beyond Repair).xlsm	Alternate calculation for 55° case at the weld centerline
	ANO1 HPI (D - Weld CL - Opposite Repair).xlsm	Alternate calculation for 180° case at the weld centerline
	ANO1 HPI (E - Butter - Repair Center).xlsm	Alternate calculation for 0° case at the butter/weld interface
	ANO1 HPI (F - Butter - Avg Over Repair).xlsm	Alternate calculation for case averaged over the repair length at the butter/weld interface
	ANO1 HPI (G - Butter - Beyond Repair).xlsm	Alternate calculation for 55° case at the butter/weld interface
	ANO1 HPI (H - Butter - Opposite Repair).xlsm	Alternate calculation for 180° case at the butter/weld interface